Molecular BioSystems

Accepted Manuscript

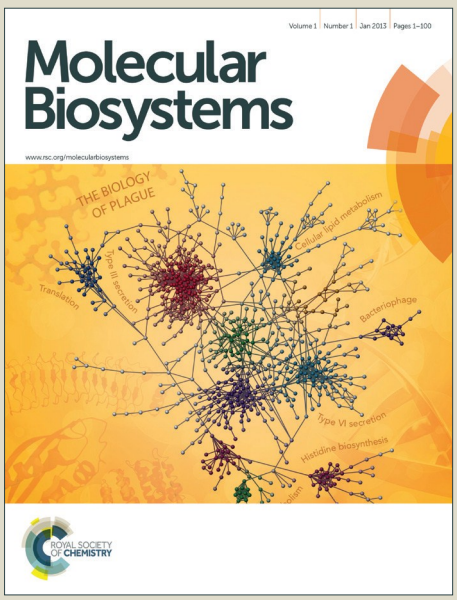

ROYAL SOCIETY OF CHEMISTRY

www.rsc.org/molecularbiosystems

In vitro and *in vivo* biological characterization of the anti-proliferative potential of a cyclic trinuclear organotin(IV) complex

Marta Martins[a], Pedro V. Baptista[b], Ana Soraia Mendo[b], Claudia Correia[b], Paula Videira[b,c], António S. Rodrigues[d], J. Muthukumaran[e], Teresa Santos-Silva[e], Ana Silva[b], M. Fátima C. Guedes da Silva[f], Joana Gigante[g], António Duarte[g], Malgorzata Gajewska[f], Alexandra R. Fernandes[b,f*]

[a]*School of Public Health, Physiotherapy and Sports Science; UCD Centre for Food Safety; Centre for Molecular Innovation and Drug Discovery; University College Dublin, Belfield, Dublin 4, Ireland.*

[b]*UCIBIO, Departamento de Ciências da Vida, Faculdade de Ciências e Tecnologias, Universidade Nova de Lisboa, 2829-516 Caparica, Portugal.*

[c]*CEDOC, NOVA Medical School / Faculdade de Ciências Médicas, Universidade Nova de Lisboa, Lisboa, Portugal .*

[d]*Centre for Toxicogenomics and Human Health , NOVA Medical School/Faculdade de Ciências Médicas, Universidade Nova de Lisboa, Lisbon, Portugal.*

[e]*UCIBIO-REQUIMTE, Departamento de Química, Faculdade de Ciências e Tecnologia, Universidade Nova de Lisboa, Caparica 2829-516, Portugal.*

[f]*Centro de Química Estrutural, Complexo I, Instituto Superior Técnico, Universidade de Lisboa, Av. Rovisco Pais, 1049-001 Lisbon, Portugal.*

[g]*Centro de Investigação Interdisciplinar em Sanidade Animal, Faculdade de Medicina Veterinária, Universidade de Lisboa, Lisboa, Portugal.*

***Corresponding author:** Alexandra R. Fernandes, UCIBIO, Departamento de Ciências da Vida, Faculdade de Ciências e Tecnologias, Universidade Nova de Lisboa, 2829-516 Caparica, Portugal. *e-mail*: ma.fernandes@fct.unl.pt

Abstract

Identification of novel molecules that can selectively inhibit the growth of tumor cells, avoiding patient side effects and/or intrinsic or acquired resistance, usually associated to common chemotherapeutic agents, is of utmost importance. Organometallic compounds have gained importance in oncologic chemotherapy, such as organotin(IV) complexes. In this study, we assessed the anti-tumor activity of the cyclic trinuclear organotin(IV) complex with aromatic oximehydroxamic acid group $(nBu_2Sn(L)]_3(H_2L$=N,2-dihydroxy-5-[N-hydroxyethanimidoyl] benzamide) - MG85 - and provide further characterization of its biological targets. We have previously shown the high anti-proliferative activity of this complex against human colorectal and hepatocellular carcinoma cell lines and a lower cytotoxicity in neonatal non-tumor fibroblasts. MG85 induces tumor cell apoptosis and downregulation of proteins related to tubulin dynamics (TCTP and COF1). Further characterization included: i) evaluation of interference in the cell cycle progression, including expression of critical genes; ii) affinity to DNA and the corresponding mode of binding; iii) genotoxic potential in cells with deficient DNA repair pathways; and iv) *in vivo* tumor reduction efficiency using mouse colorectal carcinoma xenografts.

Key words: Colorectal carcinoma; HCT116; Organotin(IV) complexes; tubulin; DNA interaction.

Introduction

There is a growing demand for compounds that can selectively inhibit tumor growth but spare healthy tissue to deleterious effects and avoid the appearance of drug resistance profiles.[1] Since the discovery of the antitumor activity of cisplatin, several metal complexes have been explored regarding their potential application in cancer treatment.[2] Metal complexes are versatile molecules due to the intrinsic characteristics of both metal centers and ligands, providing for a wide range of reactional properties (see Meggers).[3] Metal centers are prone to participate in nucleophilic substitution reactions due to their cationic nature, targeting amino acids and nucleotides,[4] and thus making proteins and nucleic acids important cellular targets. Indeed, the antitumor effect of platinum complexes is generally accepted to result from their reactivity towards DNA.[5] Nucleophilic substitution reactions result in the formation of DNA adducts or either intra- or inter-molecular crosslinking, *i.e.* covalent interactions. On the contrary, the presence of polycyclic aromatic ligands favors the establishment of three possible modes of non-covalent interaction with DNA, namely, groove binding, intercalation and insertion.[6] Some metal complexes can also participate in nucleic acid cleavage acting as artificial metallonucleases either by catalyzing direct hydrolysis[7] or oxidative cleavage by induction of reactive oxygen species (ROS).[8]

In recent years, organotin(IV) complexes have attracted considerable attention owing to their potential biocidal activity and cytotoxicity.[9–18] Cytotoxic organotin(IV) complexes with biologically active ligands, such as hydroxamic acids, have shown promising antitumor activities against MCF-7 mammary and HCT116 colon tumor cell lines.[10,11] Gajewska and collaborators synthesized and characterized a cyclic trinuclear organotin (IV) complex with aromatic oximehydroxamic acid group $(nBu_2Sn(L)]_3(H_2L$=N,2-

dihydroxy-5-[N-hydroxyethanimidoyl] benzamide) (herein referred as MG85), which presented *in vitro* anti-proliferative activity against four tumor cell lines: human promyelocytic leukemic HL-60; human hepatocellular Bel-7402; human gastric BGC-823; and human nasopharyngeal KB carcinomas.[12] We have also demonstrated the high anti-proliferative activity and cytoselectivity of the complex in colorectal HCT116, hepatocellular carcinoma HepG2 and neonatal non-tumor fibroblasts.[19] MG85 induces cell death *via* apoptosis, up-regulation of Cu/Zn superoxide dismutase (SOD1) correlating with increased levels of ROS in HCT116 cells. Proteomic analysis suggested a good therapeutic potential of MG85 by affecting the expression of proteins typically deregulated in tumors as well as a possible role in tubulin microtubules destabilization.

Here, we provide further insights into the mechanisms of biological action of this promising anticancer compound, namely, impact in cell cycle; expression of critical regulatory genes; affinity to DNA and the corresponding mode of binding, genotoxic potential in cells with deficient DNA repair pathway; interaction with tubulin; and assessment of its efficiency *in vivo*.

Experimental Section

Organotin(IV) Complex

The metal complex $[nBu_2Sn(L)]_3$ – MG85 - was synthesized and characterized as described.[12]

Cell culture

HCT116 human colorectal carcinoma, HepG2 human hepatocellular carcinoma and MCF-7 breast adenocarcinoma cell lines were grown as previously described.[20,21] MCF-10A mammary epithelial cells were grown in DMEM/F12 (Invitrogen) supplemented with 0.5 μg/mL hydrocortisone (1 mg/mL; Sigma, Spain), 5 % (v/v) donor horse serum (Sigma, Spain), 20 ng/mL epidermal growth factor (EGF; 100 μg/mL; Sigma, Spain), 100 ng/mL cholera toxin (1 mg/mL; Sigma, Spain) and 10 μg/mL insulin (10 mg/mL; Sigma, Spain). Chinese hamster pulmonary fibroblasts (V79 cells) were grown in DMEM supplemented with 5% (v/v) fetal bovine serum (Invitrogen Corp.) in 50 mL Falcon tubes tilted by 45º. All cell cultures were maintained at 37ºC in a humidified atmosphere and 5% (v/v) CO_2.

Cell viability

MCF-10A cells were seeded at 0.75×10^5 cells/mL in 96-well microplates (Corning, NY, USA). Media was removed 24 h after seeding and replaced with fresh media containing 0.01 – 1 μM of MG85 complex or 0.1 % (v/v) absolute ethanol (vehicle control). After 48 h of incubation in the presence or absence of the compound, cell viability was evaluated with CellTiter 96® AQueous Non-Radioactive Cell Proliferation Assay Kit (Promega, Madison, EUA). [20,21]

Caspase-3/-7 activity

HCT116 cells were plated at 7500 cells/well in a black opaque 96-well microplate (Corning). Media was removed 24 h after plating and replaced with fresh media containing increasing concentrations of the MG85 complex (0.10, 0.35 and 0.40 μM) or 0.1 % (v/v) absolute ethanol (vehicle control). The blank control was made with culture medium without cells. Cells were incubated for 48 h at 37ºC and 5 % CO_2. Caspase-3/-7 combined activity was quantified using the Apo-ONE® Homogeneous Caspase-3/7 Assay (Promega, Madison, WI, USA) according to the manufacturer's instructions and [22]. Briefly, 100 μL of a mixture containing the profluorescent substrate was added to each well and after an incubation period of 2 h at 37ºC and 5% CO_2, fluorescence was measured in an Anthos Zenyth 3100 (Anthos Labtec Instruments) plate reader with excitation and emission wavelengths of 485 and 535 nm, respectively.

Cell cycle analysis

HCT116 cells were plated in 25 cm^2 culture flasks with a density of $3x10^5$ cells/flask and synchronized in early S-phase by double thymidine block (2 mM), as described elsewhere.[19] Cells were released from the second block by replacing the medium with fresh medium containing 0.05 μM of MG85 or absolute ethanol (vehicle control). After incubation periods of 8 and 24 h at 37°C and 5 % (v/v) CO_2, cells were treated with propidium iodide (PI) as described.[23] Data were collected on Attune® Acoustic Focusing Flow Cytometer (Life Technologies, Carlsbad, California) and analyzed using Attune® Cytometric software (Life Technologies).

Expression analysis

HCT116 cells were plated into 25 cm^2 culture flasks at a concentration of $1x10^5$ cells/flask and incubated for 24 h at 37ºC and 5% CO_2. Culture media was replaced by fresh media containing either 0.25 μM of MG85 complex or 0.1 % (v/v) absolute ethanol (vehicle control). Cells were incubated for 48 h at 37ºC and 5% (v/v) CO_2, centrifuged and washed twice with phosphate buffered saline (PBS) 1X solution. Total RNA was extracted from the cell pellet using the SV Total RNA Isolation System (Promega) and converted into cDNA (cDNA synthesis kit, Bioline, London, UK), according to the manufacturers' specifications. Concentration and purity of RNA and cDNA were evaluated in a NanoDrop 2000 (Thermo Scientific, Waltham, MA, USA). Single stranded cDNA was used as a template for the amplification of genes involved in cell cycle and regulation of apoptosis, using the following conditions: denaturation at 94ºC for 30 s, annealing at 52-58ºC for 30 s and extension at 72ºC for 1 min, for 35 cycles. Primer sequences and annealing temperatures are indicated in Table 1. PCR products (10 μL per sample) were subjected to gel electrophoresis on a 2% (w/v) agarose gel stained with GelRed (Biotium, Hayward, CA, USA) at 110 Volts for 50 min. *RNA18S5* was used as housekeeping gene. Relative gene expression was calculated by applying the ΔΔCt method.[24]

Table 1. **Primers, annealing temperature and amplicon size of RT-qPCR reactions.**

Gene	Coded protein	Forward primer (5'-3')	Reverse primer (5´-3')	T_{Ann} (ºC)	Product size (bp)	Ref.
CDKN1A	p21	GCTTCATGCCAGCTACTTCC	AGGTGAGGGGACTCCAAAGT	52	221	This study
CCNA2	Cyclin A	ACTTTCTGCATCAGCAGCCT	GTGTCTCTGGTGGGTTGAGG	59	336	This Study
CCNB1	Cyclin B1	GCAGCAGGAGCTTTTTGCTT	CCAGGTGCTGCATAACTGGA	59	118	This Study
CDC2	CDK1	CTGGGGTCAGCTCGTTACTC	TCCACTTCTGGCCACACTTC	59	170	This study
RNA18S5	18S Ribosome major subunit	GTAACCCGTTGAACCCCATT	CCATCCAATCGGTAGTAGCG	59	151	19

Effect of MG85 complex in DNA

1. Chromosomal aberrations

Chinese hamster pulmonary fibroblasts (V79) cells were seeded in 25 cm^2 culture flasks at 10^5 cells/flask. Cells were incubated with 0.4 μM of the MG85, 0.1% (v/v) of absolute ethanol (vehicle control) and 1.5 μM Mitomycin C (MMC; positive control) for 16 h at 37ºC and 5 % (v/v) CO_2. After 14 h incubation, 10 μL of a colchicine solution (300 μg/mL; Sigma) pre-warmed at 37ºC were added to each sample and incubated for 2 h in the same conditions. Chromosomal analysis was performed as described.[23]

2. Interaction with Topoisomerase II

The ability of MG85 to inhibit topoisomerase II was determined using the Human Topoisomerase II Decatenation Kit (Inspiralis, Norwich, UK). The substrate for decatenation consists of kDNA, a complex interlinked network of catenated DNA mini circles that due to their high molecular mass cannot enter an agarose gel under normal electrophoresis conditions. In presence of a type II topoisomerase the mini circles (2.5 Kb) are released by decatenation and can be resolved at relatively high voltages. The assay was performed according to the manufacturer's instructions. Briefly, 200 ng of kDNA were incubated in Assay buffer 1X containing 1U of topoisomerase II, in absence of any complex and in presence of 1% (v/v) absolute ethanol (vehicle control); 5-100μM of MG85 complex; or 5 μM Doxorubicin (DOX; positive control), in a total reaction volume of 30 μl at 37°C for 30 minutes. Samples were then subjected to electrophoresis on a 1% (w/v) agarose gel stained with GelRed (Biotium) at 90 Volts for 1 h, photographed and analyzed using the GelAnalyzer Software (www.gelanalyzer.com).

3. Absorption spectroscopy

Interaction of MG85 with Calf Thymus DNA (CT-DNA; Invitrogen) was assessed by UV-Visible spectroscopy as described. [21,22] CT-DNA concentration in base pairs had been determinated at 260 nm in a NanoDrop2000 spectrophotometer (ThermoScientific), using an extinction coefficient of 6600 M^{-1} cm^{-1}.

4. DNA cleavage assay

pUC18 DNA was isolated from *E. coli* grown overnight in Luria-Bertani (LB; Applichem, Darmstadt, Germany) medium with 100 μg/mL ampicillin (Bioline, London, UK), at 37°C. Plasmid purification was performed using the NZYMiniprep (Nzytech, Portugal) according to the manufacturer's instructions, except for the elution step in which 50 mM Tris-HCl, 10 mM NaCl (pH 7.25) preheated at 70°C was used. DNA was quantified by spectrophotometry with NanoDrop2000. *In vitro* interaction between MG85 and DNA was performed with 200 ng of pUC18 and MG85 at different concentrations in 5 mM Tris-HCl, 50 mM NaCl buffer (pH 7.2), as previously described.[21] Cisplatin and paclitaxel were used as control drugs (50 and 100 μM).

Tubulin polymerization assay

Microtubules destabilization was assessed by absorption spectroscopy at 37ºC using the In vitro Tubulin Polymerization Assay (ET-002B-32, Écrins Therapeutics, France) according to the manufacturer´s protocol by incubating purified bovine tubulin with guanosine-5'-triphosphate (GTP) and i) 0.2 μM of MG85 compound or ii) 10 μM of paclitaxel (microtubule-stabilizing molecule) or iii) colchicine (depolymerizing compound).

***In vivo* assays**

The Ethics and Animal Welfare Committee of the Faculty of Veterinary Medicine of University of Lisbon, Portugal approved all the procedures involving animals.

i) **Her2 mice:** The transgenic Her2/NeuNDL2:5 (Her2) mice of MMTV background (neu oncogene under the transcriptional control of the mouse mammary tumor virus) were provided by William J. Muller.[25,26] The animals were housed in well-ventilated propylene cages with sawdust as bedding, in a room with controlled temperature between 22°C and 25°C and a 12-hours-light/12-hours-dark cycle. The mice were fed with standard laboratory diet and water *ad libitum.*

All Her2 mice from experimental and control groups were multiparous females. To study the effects of MG85 on the growth of Her2 mammary tumors, treatments with vehicle (PBS) and complex (0.56 mg/kg) were administered by intraperitoneal injection to Her2 females 3 times/week during 5 weeks. The treatment begun at the age of 20 weeks and the animals were sacrificed for tumor measurement, after 5 weeks. Two independent experiments were performed involving 4 animals per treatment group. The animal's mammary glands were dissected and macroscopic tumors (≥1×1 mm) were excised. The volume of the tumors was calculated using the longer (a) and shorter (b) diameters of the tumors ($V= 0.52 \times a \times b^2$). The volumes of all tumors from each mouse were summed to give the overall tumor burden per animal.

i) **Colorectal carcinoma xenografts**: Ten Balb/c scid males mice were injected with 2×10^6 HCT116 cancer cells into the flank for tumor establishment (2 weeks). Then, the mice were subdivided into two groups: i) control group (PBS+0.2 % (v/v) ethanol (vehicle control)) and ii) MG85 group (2.8 mg/kg). Both groups (n=2) were

injected intraperitoneally 3 times/week for a total of 2 weeks, after which animals were sacrificed. The volume of the tumors was measured as described above. Tissue samples were drawn from liver, kidney, spleen, bladder, brain and tumor. The weight of each sample was noted. Samples were digested by fumic HNO_3 and Sn concentration determined by inductively coupled plasma mass spectrometry (ICP-MS) analysis.

Molecular docking studies

A molecular docking study of MG85 with the crystal structure of αβ-tubulin (PDB ID: 1JFF) was carried out using Auto Dock 4.2.[27] Firstly, the three-dimensional structure of the target protein[28] was prepared by adding polar hydrogens and assigning kollman charges into PDBQT format. Subsequently, the crystal structure of MG85 was retrieved from Cambridge Crystallographic Data Centre (CCDC; accession number CCDC-729868) and then subjected into ligand preparation steps which include the addition of gasteiger charges, merging of non-polar hydrogens and setup of all rotatable bonds. In order to identify the possible binding pocket of MG85, initially, the grid map was generated around the αβ-tubulin structure (196 Å x 134 Å x 156 Å grid box size; 0.375 Å grid spacing and 95.740 Å x 79.780 Å x 5.770 Å grid center) followed by paclitaxel binding site (47 Å x 49 Å x 38 Å grid box size; 0.375 Å grid spacing and 2.160 Å x -16.810 Å x 14.510 Å grid centre). Paclitaxel was used as reference for the present study, and the corresponding three-dimensional structure was retrieved and prepared as mentioned above. In the docking calculation, the Lamarckian Genetic Algorithm (LGA) was employed with the parameters of 50 docking trials, 150 population size, 2500000 maximum number of energy evaluations, 27000 maximum number of generations, 0.02 mutation rate and 0.8 cross-over rate. Once the docking simulation was completed, the best protein-ligand complex was selected on the basis of estimated free energy of

binding (ΔG) and inhibition constant (Ki). The MGL Tools, PyMOL Version 1.3 and LigPlot+ Version 1.4.5 programs[29,30] were used for analysing and comparing the docking result with the reference molecule.

Statistical analysis

All statistical analyses were performed with Statistical Package for the Social Sciences software v17.0 (SPSS v17.0, Chicago, IL) using Mann-Whitney-Wilcoxon test, and results expressed as mean ± SEM resulting from at least three independent experiments. Statistical significance was evaluated using the Student's t-test; $p<0.05$ was considered statistically significant (indicated in the figures with *).

Results and Discussion

MG85 is a promising anticancer compound with relative cytoselectivity, showing lower cytotoxicity in human healthy fibroblasts when compared to tumor cell lines, HCT116 and HepG2. Since fibroblasts are a non-epithelial type of human cells, here we performed the viability assays in MCF-10A cells, an epithelial non-tumorigenic cell line from normal mammary gland (Supplementary Figure S1). MG85 shows a lower cytotoxicity in MCF-10A cells with an IC_{50} value of 1±0.02 μM (fibroblasts 0.538±0.047 μM), comparing to IC_{50} values for all the previously tested tumor cells of 0.238±0.011 μM (HCT116) and 0.199±0.003 μM (HepG2).[19] These data on MCF-10A cell line confirms the higher cytotoxicity towards tumor cells, particularly HCT116 and HepG2, when compared with healthy cells.

To further confirm MG85's capability to induce apoptosis in HCT116 cell line, the combined activity of the effector caspases 3/7 was determined. An increase of caspase 3 and 7 activities superior to 1.5-fold was observed for all tested concentrations when compared to control (Figure 1). These results are consistent with our previous data, flow cytometry and nuclear morphological assessment,[19] which indicated that MG85 was able to induce cell death *via* apoptosis.

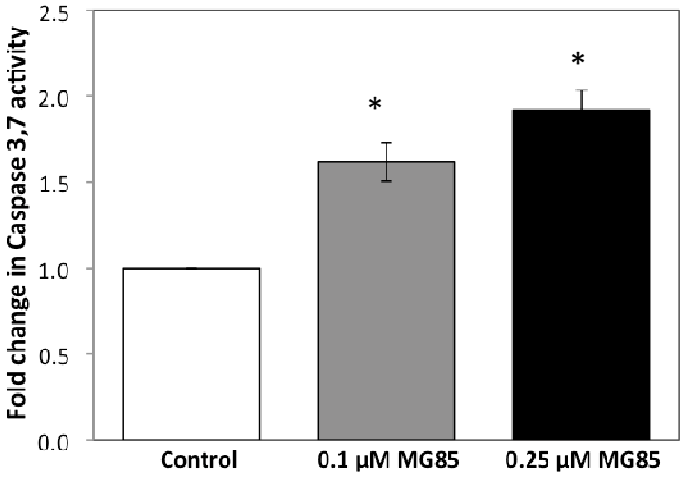

Figure 1. Activity of the effector caspases 3 and 7 in HCT116 cells after 48 h of exposure to 0.1 % (v/v) ethanol (vehicle) (white bar); 0.1 µM (grey bar); and 0.25 µM (black bar) of MG85. Data are the mean ± SEM percentage compared to control from three independent experiments. * $p < 0.05$ was considered statistically significant.

To further clarify the mechanisms of cytostatic potential promoted by MG85, cell cycle progression of untreated and MG85-treated HCT116 cells (for 4h and 8h) was evaluated by flow cytometry using propidium iodide (PI) labeling (Figure 2). A significant delay of the cell cycle is observed between 4h and 8h. At 4h, MG85-treated cells are mainly in S phase while control cells progressed to G2/M. At 8 h, the majority of MG85-treated cells are at G2/M and untreated cells progressed to G1.

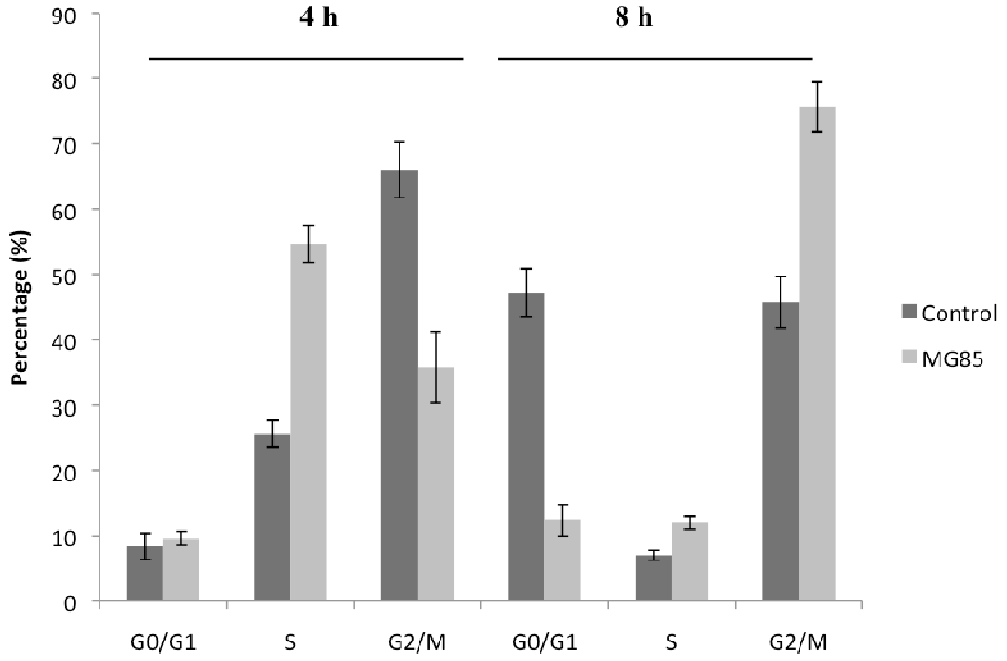

Figure 2. Flow cytometry analysis of HCT116 cells stained with PI and treated with MG85 (0.25 μM) and absolute ethanol (vehicle control) for 4 h and 8 h. Percentage (%) of cells in G0/G1, S and G2/M is depicted. Data values are the mean ± SEM percentage from three independent experiments. PI, Propidium Iodide; h, hours.

Considering the impact in the cell cycle, we evaluated the expression levels of several key genes involved in cell cycle regulation. Indeed, HCT116 cells exposed to MG85 express higher levels of *CDKN1A* gene that codes for p21, an inhibitor of cell cycle progression (Figure 3). These gene expression data are in agreement with the cell cycle analysis attained by flow cytometry, both indicating a delay in progression of the cell cycle towards M phase after incubation with MG85. Increased expression of p21 usually results in G_1/S arrest and leads to effective suppression of tumor growth *in vitro* and *in vivo*.[31,32] Studies on 14-3-3σ and p21 double-knockout cells established a complementary role of both proteins in G_2/M arrest following DNA damage.[33] Vidal

and Koff also showed that, in addition to arresting cells in G_1, p21 may inhibit Cdc2–cyclin B complexes[34] and proliferating cell nuclear antigen (PCNA),[35] preventing interaction of the latter with other components of the DNA polymerase complex. One or both of these actions might contribute to a G_2 arrest following ectopic p21 expression or DNA damage.[36–38]

MG85 may also have an impact in up-regulation of Cu/Zn superoxide dismutase (SOD1) due to higher levels of production of ROS in HCT116 cells exposed to the complex and a down regulation of proteins associated with tubulin dynamics.[19] Tubulin microtubule destabilization and increased oxidative stress correlate with cell cycle delay. Indeed, delaying cell cycle progression might allow for damage repair at the end of S phase and G_2/M checkpoints.[39,40] Also, tumor cells delayed in G_2/M may undergo apoptosis in the presence of MG85, which is in agreement with data from regulation associated to Caspase 3/7 (Figure 1).

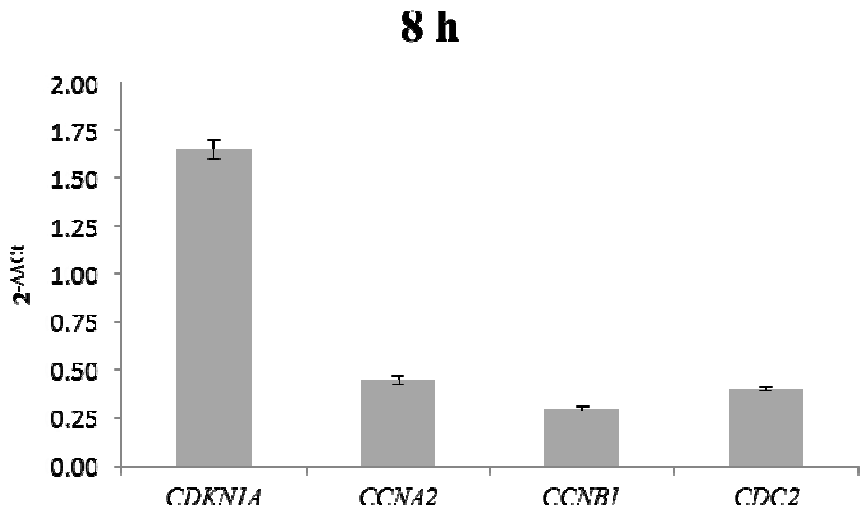

Figure 3. Relative expression levels of *CDKN1A*, *CCNA2*, *CCNB1* and *CDC2* in HCT116 cells exposed to 0.25 μM of MG85 for 8 h. Values are the mean of at least three independent experiments. Error bars represent standard deviation of the mean.

Interaction of MG85 with DNA

The binding mode of MG85 with CT-DNA was investigated using the absorption spectra. The absorption intensity of a complex is increased (hyperchromism) upon increasing the concentration of CT-DNA due to degradation of the DNA double - helix structure.[41] The extent of the hyperchromism is indicative of the partial or non-intercalative binding modes, such as electrostatic forces, van der Waals interaction, dative bonds, hydrogen bonds and hydrophobic interaction.[41]

The UV-Vis spectra of the MG85 complex exhibited n→π*or π→π* charge transfer bands at 240-340 nm (supplementary Figure S2). In the presence of increasing concentrations of CT-DNA, the complex exhibited hyperchromism with almost no shifts at 260 nm, and without a shift at n→π*or π→π* charge transfer bands which indicated that the complex binds to DNA by non-intercalative modes. The changes in absorbance with increasing amounts of CT-DNA were used to evaluate the intrinsic binding constant K_b for the MG85 complex. The intrinsic binding constant K_b was calculated[22,23] by plotting [DNA/(ε_a-ε_f)] *vs* [DNA]) and monitoring the changes in the π-π* or n- π* charge transfer bands with increasing concentration of CT-DNA and was observed as $2.55 \pm 0.05 \times 10^4$ mol^{-1}.L. This value is of the same order of magnitude of other metal complexes that bind DNA by non-intercalative modes.[42]

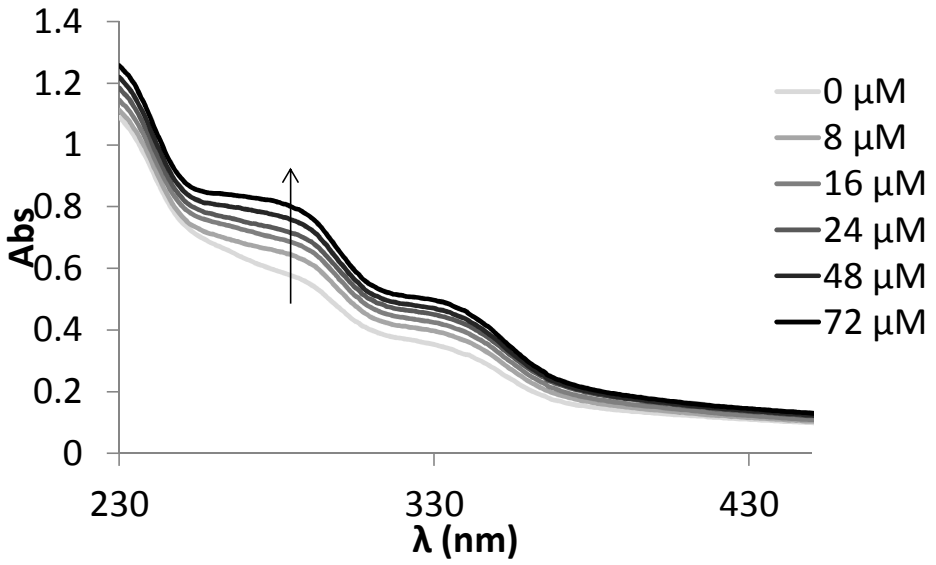

Figure 4. UV spectra of MG85 (45 μM) in the absence (light grey line) and presence (black lines) of increasing amounts of CT-DNA. The arrow indicates the variation of absorption with increasing DNA concentrations (0 to 72 μM). The dashed line represents the spectrum for the highest DNA concentration. Abs – Absorbance. λ – wavelenght.

In vitro incubation of MG85 with pDNA did not show induction of single/double strand breaks (Supplementary Figure S3). However, considering the cell cycle arrest at the end of S phase and G_2/M checkpoints, we evaluated the MG85 genotoxic potential *via* analysis of chromosomal aberrations in V79 cells. Endoreduplication, *i.e.* replication of chromosomes without subsequent cell division, was observed in cells treated for 16 h with 0.4 μM of MG85. This type of aberration is confirmed by the presence of diplochromosomes in 34% of the cells (Figure 5). These data indicate a possible interference of the complex either with mitotic spindle proteins or with topoisomerase II.

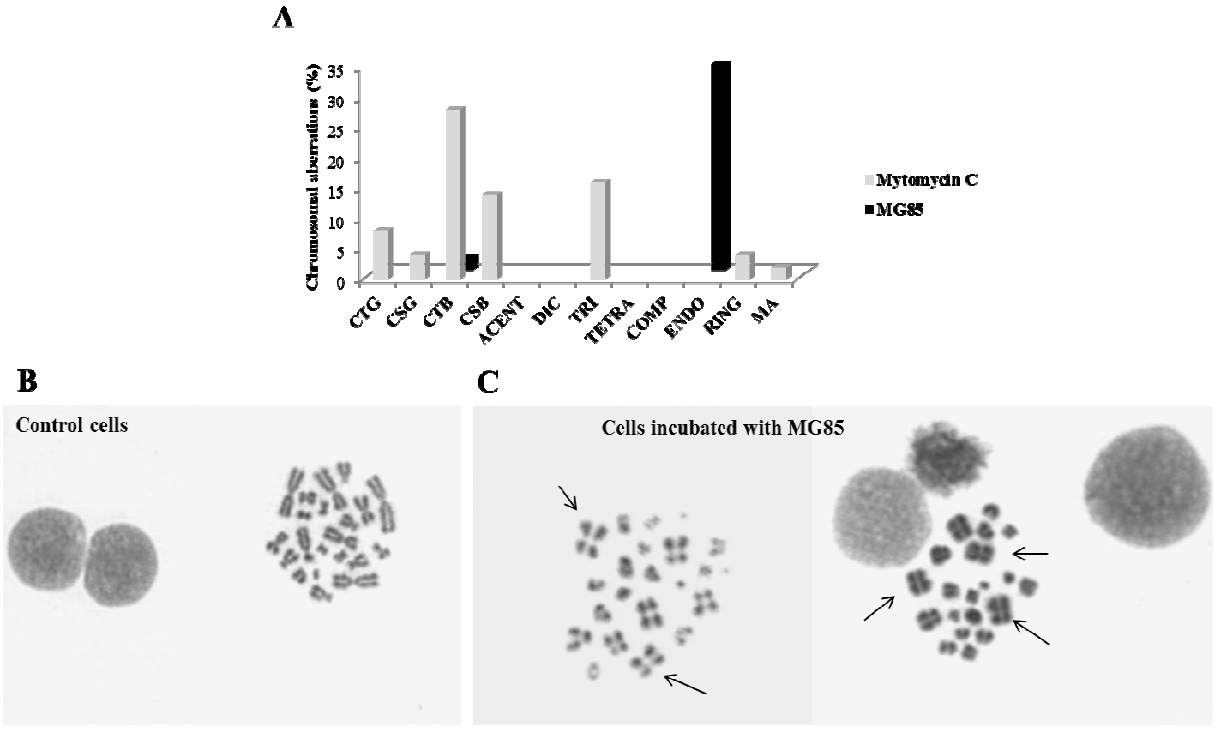

Figure 5. (A) Induction of chromosomal aberrations on V79 cells after a 16 h exposure to 1.5 μM mytomycin C (grey bars) and 0.4 μM MG85 complex (black bars). CTG: Chromatid gap; CSG: Chromosome gap; CTB: Chromatid break; CSB: Chromosome break; ACENT: Acentric Chromosome; DIC: Dicentric chromosome; TRI: Triradial chromosome; TETRA: Tetraradial chromosome; RING: Ring chromosome; MA: Cells with multi-aberrant chromosomes; ENDO: Endoreduplication. (B and C) Metaphase plates showing normal chromosomes in control cells (B) and diplochromosomes (indicated by arrows) in cells incubated with 0.4μM of the MG85 complex (C).

Due to the endoreduplication observed in V79 cells in the presence of MG85 we tested its ability to inhibit topoisomerase II activity[43,44] using high molecular weight catenated DNA, which consists in interlinked DNA circles that are released during enzymatic reaction. Incubation of catenated DNA with increasing concentrations of MG85 showed

that topoisomerase II was capable to resolve these structures for all tested concentrations - Figure S4. One may assume that most likely inhibition of topoisomerase II is not the mechanism by which MG85 induces nuclear aberrations.

Taken together, the capability of MG85 to induce endoreduplication in V79 cells (Figure 5), cell cycle delay at G2/M checkpoint (Figure 2) and down regulation of proteins associated with tubulin dynamics[19] point out a role for MG85 in altering tubulin polymerization or depolymerization. Such interaction is usually associated to the chemotherapeutic paclitaxel (PTX), which induces apoptosis following G_2/M arrest due to microtubule disorganization triggering apoptotic cell death.[44,45] Also, PTX-induced G_2/M accumulation in sarcoma cells was reduced by overexpression of $p21^{waf1}$, whereas a larger fraction of $p21^{waf1}$-induced cells remained in S-phase after treatment with PTX.[45] Niculescu *et al*[45] also reported that $p21^{waf1}$ induction may cause DNA endoreduplication in pRb-negative cells. Therefore, we explored a possible role of MG85 in tubulin polymerization *via* an *in vitro* tubulin polymerization assay (Figure 6). Indeed, MG85 induces microtubule structure stabilization, though at a lesser extent than for PTX, observed by an increase in absorbance when compared to control.

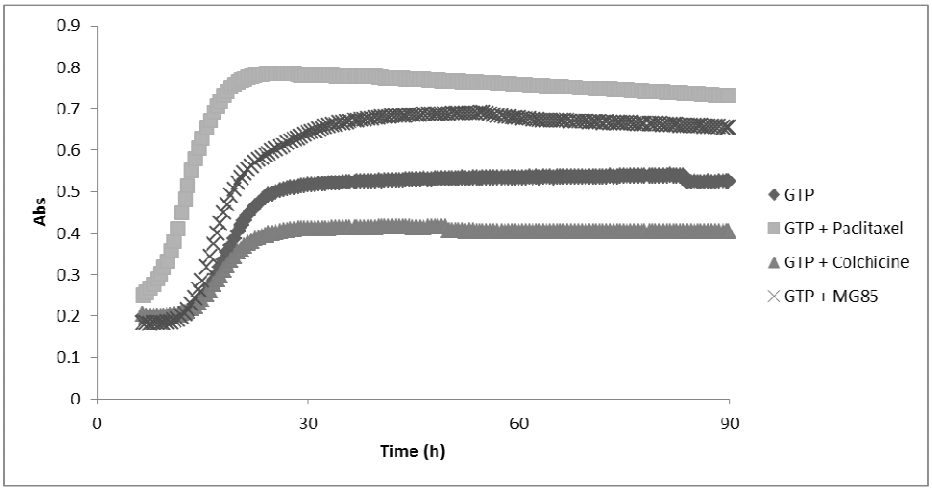

Figure 6. Tubulin destabilization assessment absorbance spectroscopy using the *in vitro* tubulin polymerization assay with 0.2 μM MG85 and 10 μM of paclitaxel and colchicine (mitotic spindle blocker). Results are the mean of three independent experiments. Abs – Absorbance.

In silico interaction studies were carried out to predict the binding orientation of MG85 with αβ-tubulin from *Bos taurus* (PDB ID: 1JFF) and to explore the detailed intermolecular interactions and probable binding mode of the organometallic molecule. First, a blind docking calculation was performed in order to identify the possible binding sites of MG85 in the target protein. The results suggested that MG85 might bind un-specifically at the surface of the β subunit (I), at the interface between α and β subunits (II) and at the paclitaxel-binding site (III), also in the β subunit. From all possible conformations obtained, none was occupying the colchicine-binding site (see Figure 8). Using paclitaxel as a reference, free energy of binding (ΔG) and inhibition constant (Ki) were computed. Molecular docking data suggested that, in comparison with reference molecule (ΔG: -10.00 kcal/mol and Ki: 46.43 nM), MG85 showed significant binding free energy and strong binding affinity towards β-tubulin (-11.37 kcal/mol, Ki: 4.62 nM). As with paclitaxel, Val23, Leu217, His229, Ser277, Pro360,

Gly370 and Leu371 residues of β-tubulin are involved in hydrophobic interactions with MG85. Furthermore, main chain atoms of Glu22 and Arg278 are also hydrogen bonded to oxime groups of MG85 with predicted bond distances of 2.6 Å and 2.9 Å, respectively. These putative interactions may account for the strong binding of MG85 to αβ-tubulin at the paclitaxel-binding site, corroborating the experimental results here reported.

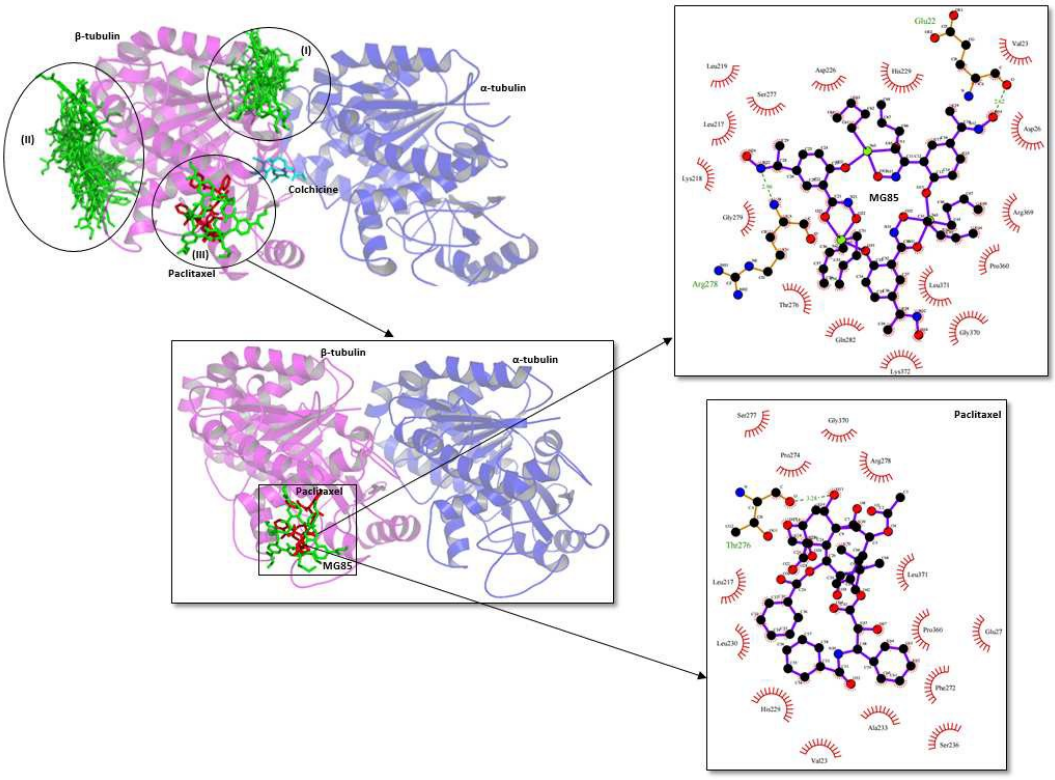

Figure 8. Predicted binding orientation of MG85 (green sticks) superimposed with the crystal structure of *Bos taurus* αβ-tubulin bound to paclitaxel (red sticks) (PDB ID: 1JFF). Colchicine is represented in cyan. Highlighted are the amino acid residues of αβ-tubulin around the ligand molecule with putative hydrogen bonds and hydrophobic contacts (distances in Å).

Molecular dynamics simulations by Mitra et al. suggest that the binding of paclitaxel to the M-loop leads to its flexibility decrease and induces conformational changes of

surrounding loops located at the interface between protofilament monomers. These short and long-range changes may facilitate the interaction between neighboring dimers, microtubules' structure stabilization and the formation of abnormal bundles of microtubules. This all results in a strong interference of mitosis.[46] The docking results here obtained suggest the formation of a similar protein-ligand complex, which could lead to the similar local and allosteric changes, promoting intermolecular stabilizing effects.

MG85 potential as an anti-cancer drug strongly relies on its high anti-proliferative activity that compares positively to known antitumor agents, such as DOX;[19] and induction of microtubule stabilization as a mode of action. To assess MG85 potential *in vivo*, we used Her2 mice (spontaneous model of murine mammary tumors) treated 3 times per week with 1.1 mg of MG85/kg for a total of 5 weeks. A 17 % reduction of the mammary tumor burden was observed following treatment (Figure 7A). MG85 was also capable of inhibiting tumor growth in Balb/c scid HCT116-xenografted mice. HCT116 xenografts were treated with 2.8 mg of MG85/Kg 3 times per week during 2 weeks. Data shows a market 90 % reduction of tumor growth (Figure 7B).

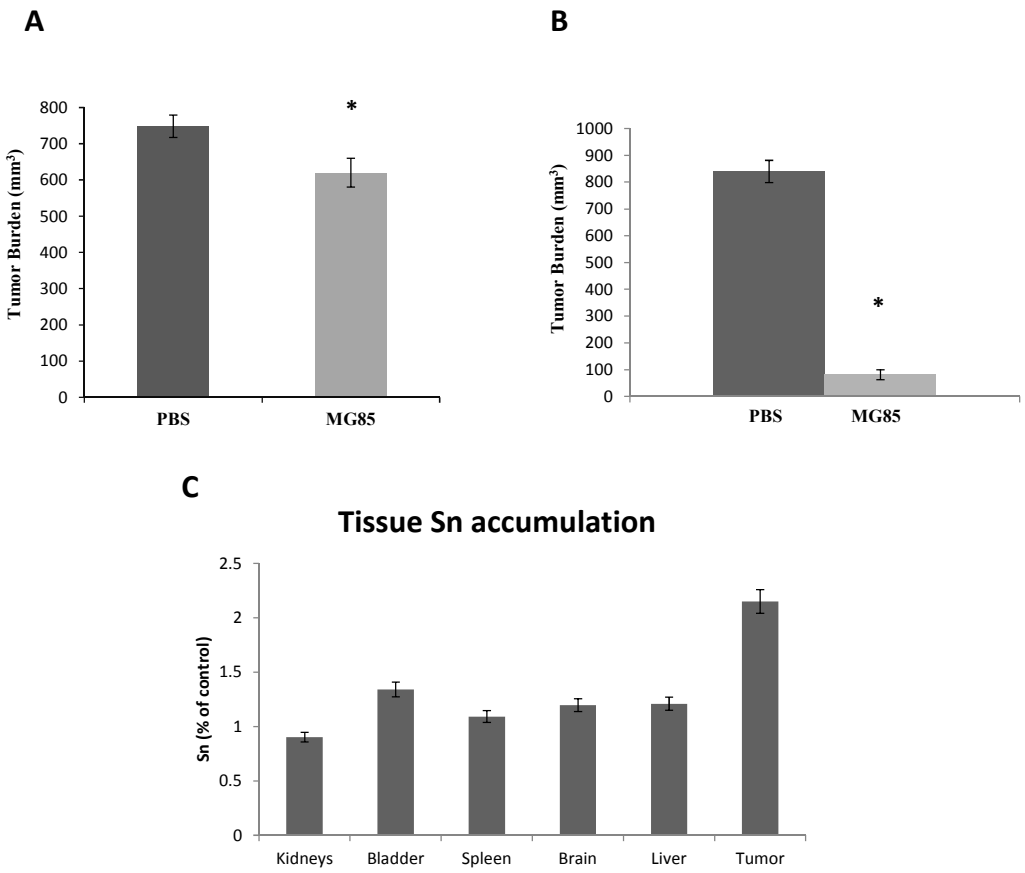

Figure 7A. MG85 inhibition of mammary tumor growth in Her2 mice. Overall tumor burden was calculated as the sum of tumor volumes per mouse in Her2 mice treated with drug vehicle (PBS, n=4) or complex (n=4). Data was analyzed using the Mann-Whitney-Wilcoxon test. Error bars represent SEM. * $p < 0.05$ considered significant. **B.** Inhibition of the tumor growth in Balb/C scid xenografted mice (n=3) after MG85 treatment. Tumor burden was determined by the sum of tumor volumes per mouse, in Balb/C scid xenografted mice treated with drug vehicle (PBS+0.2% EtOH) or the Sn(IV) complex. **C**. Sn (% of control) in Balb/c scid xenografted mice tissues based on ICP-MS. All the results are expressed as the mean ± SEM.

Although these *in vivo* results are preliminary they clearly follow the previous *in vitro* results[19] with HCT116 colorectal carcinoma cells demonstrating to be more sensitive to the MG85 complex (IC_{50} 0.238±0.011 μM) compared to breast adenocarcinoma (MCF-7) cells (IC_{50} 0.477 ± 0.019 μM) (Figures 7A and B). Moreover, as observed in Figure 7C there is an increased accumulation of Sn in tumor samples compared to the other tissue, particularly kidney, brain, liver and spleen.

Conclusions

In this study, we assessed the anti-tumor activity of the cyclic trinuclear organotin(IV) complex with aromatic oximehydroxamic acid group (nBu2Sn(L)]3(H2L=N,2-dihydroxy-5-[N-hydroxyethanimidoyl] benzamide) - MG85. We show that MG85 induces cell death by apoptosis with an increase of at least 1.6-fold on the effector caspases 3/7 activities. MG85 selectivity towards tumor cell lines, particularly HCT116 and HepG2, was demonstrated by the significantly lower loss of viability in non-tumorigenic epithelial cells when compared to tumor cells. The observed increase in expression of *CDKN1A*, and lower expression of *CCNA2*, *CCNB1* and *CDC2*, associated to the observable cell cycle delay in late S phase and G_2/M checkpoint, seems to be the cell's machinery attempt to repair the MG85 induced genotoxic damages, such as the presence of diplochromosomes in 34% of treated cells and stabilization of tubulin polymerization to prevent asymmetrical distribution of chromosomes.[25] If damage repair is not adequate, the cell will undergo apoptosis. Also, MG85 seems to interact with CT-DNA by a groove-binding mechanism within the same order of magnitude of that of doxorubicin-DNA affinity constant.

The preliminary data on the anti-tumor activity of this organotin(IV) complex, particularly in reducing colorectal carcinoma tumors, clearly deserves further attention. Novel solutions for the active targeting of such compounds may provide an increased trend of therapeutic potential reducing toxicity towards normal cells.

Acknowledgements

We thank FCT/MEC for financial support (PTDC/BBB-NAN/1812/2012; PTDC/QUI-BIQ/117799/2010; SFRH/BPD/97719/2013; PEst-OE/QUI/UI0100/2013; UID/Multi/04378/2013). We also thank AJL Pombeiro, J. Silva, D. Luis, G. Cabral (CEDOC, FCM/UNL) and C. Carvalho for technical support and S. Santos for preliminary discussions.

References

1 D. L. Wheeler, S. Huang, T. J. Kruser, M. M. Nechrebecki, E. A. Armstrong, S. Benavente, V. Gondi, K.-T. Hsu and P. M. Harari, *Oncogene*, 2008, **27**, 3944–3956.

2 M. Hannon, *Pure Appl. Chem.*, 2007, **79**, 2243–2261.

3 E. Meggers, *Chem. Commun. (Camb).*, 2009, 1001–1010.

4 C. X. Zhang and S. J. Lippard, *Curr. Opin. Chem. Biol.*, 2003, **7**, 481–489.

5 G. Cantero, N. Pastor, S. Mateos, C. Campanella and F. Cortés, *Mutat. Res. - Fundam. Mol. Mech. Mutagen.*, 2006, **599**, 160–166.

6 B. M. Zeglis, V. C. Pierre and J. K. Barton, *Chem. Commun. (Camb).*, 2007, **7345**, 4565–4579.

7 N. H. Williams, B. Takasaki, M. Wall and J. Chin, *Acc. Chem. Res.*, 1999, **32**, 485–493.

8 Q. Jiang, N. Xiao, P. Shi, Y. Zhu and Z. Guo, *Coord. Chem. Rev.*, 2007, **251**, 1951–1972.

9 M. Gielen, and E. R. T. Tiekink, in *Metallotherapeutic Drugs & Metal-Based Diagnostic Agents: The Use of Metals in Medicine*, ed. E. R. T. Gielen, M. and Tiekink, Chichester, UK, John Wiley., 2005, pp. 421–439.

10 Q. Li, M. F. C. G. da Silva and A. J. L. Pombeiro, *Chemistry*, 2004, **10**, 1456–1462.

11 X. Shang, J. Cui, J. Wu, A. J. L. Pombeiro and Q. Li, *J. Inorg. Biochem.*, 2008, **102**, 901–909.

12 M. Gajewska, K. V Luzyanin, M. F. C. Guedes Da Silva, Q. Li, J. Cui and A. J. L. Pombeiro, *Eur. J. Inorg. Chem.*, 2009, 3765–3769.

13 M. S. Ahmad, M. Hussain, M. Hanif, S. Ali and B. Mirza, *Molecules*, 2007, **12**, 2348–2363.

14 A. Alama, B. Tasso, F. Novelli and F. Sparatore, *Drug Discov. Today*, 2009, **14**, 500–508.

15 C. Yan, Zhang J, Liang T and L. Q, *Biomed Pharmacother*, 2015, **71**, 119–127.

16 M. Nath, M. Vats and P. Roy, *J. Photochem. Photobiol. B.*, 2015, **148**, 88–100.

17 M. Sirajuddin, S. Ali, V. McKee, M. Sohail and H. Pasha, *Eur. J. Med. Chem.*, 2014, **84**, 343–63.

18 R. A. Khan, S. Yadav, Z. Hussain, F. Arjmand and S. Tabassum, *Dalt. Trans*, 2014, **43**, 2534–2548.

19 A. Silva, D. Luís, S. Santos, J. Silva, A. S. Mendo, L. Coito, T. F. S. Silva, M. F. C. Guedes Da Silva, L. M. D. R. S. Martins, A. J. L. Pombeiro, P. M. Borralho, C. M. P. Rodrigues, M. G. Cabral, P. A. Videira, C. Monteiro and A. R. Fernandes, *Drug Metabol. Drug Interact.*, 2013, **28**, 167–176.

20 T. F. S. Silva, P. Smoleński, L. M. D. R. S. Martins, M. F. C. Guedes Da Silva, A. R. Fernandes, D. Luis, A. Silva, S. Santos, P. M. Borralho, C. M. P. Rodrigues and A. J. L. Pombeiro, *Eur. J. Inorg. Chem.*, 2013, 3651–3658.

21 T. F. S. Silva, L. M. D. R. S. Martins, M. F. C. Guedes da Silva, A. R. Fernandes, A. Silva, P. M. Borralho, S. Santos, C. M. P. Rodrigues and A. J. L. Pombeiro, *Dalton Trans.*, 2012, **41**, 12888–12897.

22 D. V. Luís, J. Silva, A. I. Tomaz, R. F. M. De Almeida, M. Larguinho, P. V. Baptista, L. M. D. R. S. Martins, T. F. S. Silva, P. M. Borralho, C. M. P. Rodrigues, A. S. Rodrigues, A. J. L. Pombeiro and A. R. Fernandes, *J. Biol. Inorg. Chem.*, 2014, **19**, 787–803.

23 J. Silva, A. S. Rodrigues, P. A. Videira, J. Lasri, A. J. Charmier, A. J. L. Pombeiro and A. R. Fernandes, *Inorganica Chim. Acta*, 2014, **423, Part** , 156–167.

24 T. D. Schmittgen and K. J. Livak, *Nat. Protoc.*, 2008, **3**, 1101–1108.

25 E. R. Andrechek, W. R. Hardy, P. M. Siegel, M. A. Rudnicki, R. D. Cardiff and W. J. Muller, *Proc. Natl. Acad. Sci. U. S. A.*, 2000, **97**, 3444–3449.

26 C. Dumontet and M. A. Jordan, *Nat Rev Drug Discov*, 2010, **9**, 790–803.

27. G. M. Morris, D. S. Goodsell, R. S. Halliday, R. Huey, W. E. Hart, R. K. Belew, A. J. Olson and M. E. T. Al, *J. Comput. Chem.*, 1998, **19**, 1639–1662.

28 J. Löwe, H. Li, K. H. Downing and E. Nogales, *J. Mol. Biol.*, 2001, **313**, 1045-1057.

29 The PyMOL Molecular Graphics System, Version 1.7.4 Schrödinger, LLC.

30 R. A. Laskowski and M. B. Swindells, *J. Chem. Inf. Model.*, 2011, **51**, 2778–2786.

31 A. L. Gartel, M. S. Serfas and A. L. Tyner, *Proc. Soc. Exp. Biol. Med.*, 1996, **213**, 138–149.

32 T. Abbas and A. Dutta, *Nat. Rev. Cancer*, 2009, **9**, 400–414.

33 T. A. Chan, H. Hermeking, C. Lengauer, K. W. Kinzler and B. Vogelstein, *Nature*, 1999, **401**, 616–620.

34 A. Vidal and A. Koff. *Gene*, 2000, **247**, 1–15.

35 S. Waga, G. J. Hannon, D. Beach and B. Stillman, *Nature*, 1994, **369**, 574–578.

36 A. L. Blajeski, V. A. Phan, T. J. Kottke and S. H. Kaufmann, *J. Clin. Invest.*, 2002, **110**, 91–99.

37 C. Cayrol, M. Knibiehler and B. Ducommun, *Oncogene*, 1998, **16**, 311–320.

38 F. Bunz, A. Dutriaux, C. Lengauer, T. Waldman, S. Zhou, J. P. Brown, J. M. Sedivy, K. W. Kinzler and B. Vogelstein, *Science*, 1998, **282**, 1497–1501.

39 M. C. Hollander and A. J. J. Fornace, in *DNA Repair Mechanisms: Impact on Human Diseases and Cancer.*, ed. J. H. Vos, Landes, Austin, TX, 1995, pp. 221–237.

40 N. I. Dmitrieva, L. F. Michea, G. M. Rocha and M. B. Burg, in *Comparative Biochemistry and Physiology - A Molecular and Integrative Physiology*, 2001, vol. 130, pp. 411–420.

41 S. Tysoe and R. Morgan, *J. Phys.,* 1993, **2**, 1707–1711.

42 F. Cortés, S. Mateos, N. Pastor and I. Domínguez, *Life Sci.*, 2004, **76,** 121–135.

43 K. Bhalla, A. M. Ibrado, E. Tourkina, C. Tang, M. E. Mahoney and Y. Huang, *Leukemia*, 1993, **7**, 563–568.

44 K. N. Bhalla, *Oncogene*, 2003, **22**, 9075–9086.

45 A. B. Niculescu, X. Chen, M. Smeets, L. Hengst, C. Prives and S. I. Reed, *Mol. Cell. Biol.*, 1998, **18**, 629–643.

46 A. Mitra, D. Sept. *Biophys J,* 2008, **95**, 3252-3258.